6

Diversifying cerebellar impact on thalamic nuclei

Submitted to Cell Reports:

S.V. Gornati*, C.B. Schäfer*, O.H.J. Eelkman Rooda, A. Nigg,
C.I. De Zeeuw and F.E. Hoebeek

The cerebellum plays a role in coordination of movements and possibly also non-motor functions. Cerebellar nuclei (CN) axons connect to various parts of the thalamo-cortical network, but detailed information on the characteristics of cerebello-thalamic connections is lacking. Here, we assessed the cerebellar input to the ventrolateral (VL), ventromedial (VM) and centrolateral (CL) thalamus. Confocal and electron microscopy showed an increased density and size of CN axon terminals in VL compared to VM or CL. Electrophysiological recordings in vitro revealed that optogenetic CN stimulation resulted in enhanced charge transfer and action potential firing in VL neurons compared to VM or CL neurons, despite that the paired-pulse ratio was not significantly different. Together these findings indicate that the impact of CN input onto neurons of different thalamic nuclei varies substantially, which highlights the possibility that cerebellar output differentially control various parts of the thalamo-cortical network.

6.1 Introduction

Cerebellar best-known functions are involved in coordinating motor activities. It contributes for example to learning new motor skills and prediction of the sensory consequences of action [290, 359, 360]. The anatomical connections that underlie this broad impact include cerebellar axons to premotor centers in the brainstem, like the red nucleus and the thalamic complex [89, 348, 361-366]. The glutamatergic projection neurons from cerebellar nuclei (CN) are known to connect to a wide range of thalamic regions encompassing primary relay nuclei, i.e. 'core nuclei', like the ventrolateral (VL) nucleus, but also association nuclei such as the ventromedian (VM) nucleus, i.e., a 'matrix nuclei', as well as intralaminar nuclei [86]. Single axon reconstructions of cerebellar-recipient zones within VL and VM reveal that although both of these nuclei connect to motor and pre-motor cortices, their axons also spread throughout other regions [367, 368]. The diffuse character of the cerebellar input on thalamo-cortical networks is further highlighted by the divergent CN-projections to the intralaminar thalamic nuclei, like the centromedian, parafascicular and centrolateral (CL) nuclei [84, 89, 308] which are considered to project non-specifically throughout cortical regions and layers [369-372].

Apart from their connectivity, neurons in thalamic nuclei are also characterized by a heterogenic dendritic morphology. For instance, the cerebellar recipient zones of the VL and VM have been shown to contain neurons with 'bushy' dendrites [367, 368, 373-375] and thereby have a different appearance than CL neurons that show polarized dendritic branching [370]. Besides the difference in the cytoarchitecture, thalamic cells have been found to show different neurochemical profiles. For instance, a subpopulation of VM cells express elevated levels of calbindin, whereas intralaminar neurons show also parvalbumin-immunoreactivity [367, 376-379]. This variability in the neurochemical and morphological aspects of thalamic neurons in the cerebellar-recipient nuclei suggests that the impact of cerebellar output on thalamic neurons varies for each target nucleus.

Due to its divergent nature, the thalamo-cortical projection is likely to affect a multitude of functions [349, 367, 380, 381]. As a consequence, cerebellar lesions can result in a wide range of symptoms that span both the motor and non-motor domains [382-384]. Cerebellar-specific mutations affect not only the motor coordination, but also the social interaction between mice [385, 386]. Several *in vivo* experiments recently showed that manipulating the cerebellar output affects sensorimotor integration by somatosensory and motor cortices and thereby could direct the thalamo-cortical activity related to voluntary movements [90, 387]. Cerebellar projections to VL and VM nuclei might also influence motor preparation and movement initiation [388]. Moreover, a recently uncovered pathway from CN to the thalamic CL neurons enables short-latency control of striatal activity [256].

So far, the electrophysiological studies that investigated the cerebello-thalamic projections focused on the VL nucleus. It has been established that mono-synaptic responses evoked by CN axon stimulation results exclusively in excitatory responses in VL neurons [90-92, 380, 387, 389]. In order to elucidate how the cerebellar impact on thalamic neurons correlates to the specific nuclei we studied the postsynaptic responses to cerebellar stimulations using *in vitro* whole cell recordings. We focused on neurons in the VL, VM and CL and correlated the electrophysiological data to the morphological and cytological details of the target neurons. Our results show that both pre- and post-synaptic aspects of the cerebello-thalamic transmission vary between these thalamic nuclei and thereby provide the first evidence for the functional diversification of the cerebellar impact on thalamo-cortical networks.

6.2 Experimental procedures

6.2.1 Animals

All experiments were performed in accordance with the European Communities Council Directive. Protocols were reviewed and approved by the Dutch national experimental animal committees (DEC) and every precaution was taken to minimize stress, discomfort and the number of animals used. Data were collected from 21-56 day old C57BL/6NHsd mice of both sexes, which were purchased from Envigo laboratories (Horst, Netherlands).

6.2.2 Virus injections

We performed stereotaxic injections of adeno-associated virus carrying Channelrhodopsin2 AAV2-hSyn-ChR2(H134R)-EYFP into CN at 2 mm anterior-posterior and 1.5-2 mm medial-lateral to lambda. For localization of the injection sites 40 µm thick horizontal sections were obtained on a freezing microtome. The tissue was incubated with DAPI (300nM). Sections where rinsed and mounted on glass.

6.2.3 Electrophysiological recordings in slices and optogenetics

Electrophysiological recordings in coronal or horizontal slices were performed at 34 ± 1˚C aCSF 40 min after dissection. Internal solution was supplemented with biocytin for morphological reconstruction. Full-field optogenetic stimulation (1 ms, 470 nm peak excitation, 0.1 to 6.65 mW/mm^2) was generated using a Polygon4000 (Mightex, Toronto, Canada) or a pE2 (CoolLED, Andover, UK). Pharmacology experiments were assessed adding AMPA- (10 µM NBQX), NMDA- (10 µM APV), mGluR1- (10 µM JNJ-16259685) and mGluR5- (50 µM MPEP) blockers to the aCSF.

6.2.4 Immunofluorescence and reconstruction

To visualize the recorded neurons and CN terminals, slices were stained for Streptavidin-Cy3 (Jackson Immunoresearch) and vGluT2 anti-guinea pig Cy5 (Millipore Bioscience Research Reagent). Using custom-written Fiji-scripts (ImageJ) we identified putative synaptic contacts that were isolated and morphologically studied using a LSM 700 microscope (Carl Zeiss). Stack's subsets of the connection were deconvolved using Huygens software (Scientific Volume Imaging) and the volume measured using a custom-written Fiji macro. To quantify the distance from soma for vGluT2-positive CN terminals we calculated the distance in 3 dimensions (using x-, y-, z-coordinates) between the center of the terminal and the center of the soma by Pythagorean Theorem. To determine the dendritic arborization of biocytin filled cells, we used the 3D Sholl analysis macro implemented in Fiji software [390].

6.2.5 Electron microscopy

Ultrastructural morphology was analyzed using electron microscope (CM 100, Philips). Staining for DAB and preparation of ultrathin section was performed as previously described [319].

6.3 Data analysis and statistics

All numerical values are given as means and error bars are SEM. Parametric and non-parametric tests were chosen as appropriate and were reported in figure legends. Data analyses were performed using SPSS 22.0 software package.
Detailed experimental procedures and statistical analyses for each experiment can be found in Supplemental Experimental Procedures.

6.4 Results

6.4.1 Thalamic nuclei receive various densities of CN axons and terminals

To assess the innervation of VL, VM and CL thalamic nuclei by cerebellar axons in the mouse brain, we transfected neurons in the interposed and lateral CN with a virally encoded YFP-expressing construct (**Figure 1A**). We found the level of intensity in the VL (55.9 ± 8.0 a.u.) to be highest compared to VM (38.7 ± 3.9 a.u.) and CL (25.8 ± 2.3 a.u.) (p=0.529 for VL *vs* VM; p=0.002 for VL *vs* CL, p=0.136 for VM *vs* CL, K-W tests, Dunn's correction; **Figure 1B** and **Online Table S1**).

In order to establish whether the regional variability in fluorescence also reflects a variable size and density of CN axon terminals, we next evaluated tissue samples that were additionally stained for vGluT2, a widely used marker to selectively label glutamatergic terminals [248, 367, 379, 391, 392]. High–magnification confocal microscopic images and custom-written image analysis scripts revealed that the VL nucleus was most densely populated by CN terminals (total count 499 terminals; N=5 mice; **Figure 1C-D**) with a mean volume of 12.45±0.74 μm^3. As previously reported [348], VM is mostly a region where cerebellar fibers pass through by sending some branches in the most medial part of the nucleus (**Figure 1E**). The number of vGLUT2 positive terminals was lower compared to VL and their size was significantly smaller (6.65±0.71 μm^3 mean value for 172 terminals isolated, $p<0.0001$, K-S test; **Figure 1F,I** and **Table S1**). The centrolateral nucleus showed the lowest number of terminals and the volume was statistically different from VL but not VM (73 terminals with mean volume size of 5.85±0.9 μm^3; p=0.0002 for VL vs CL and p=0.966 for VM vs CL, K-S test; **Figure 1G-I** and **Table S1**). Moreover we could observe a significantly higher density of vGluT2-positive CN terminals compared to CL (p=0.024; K-W test), whereas the differences in density between VL-VM and VM-CL were not significantly different (p=0.334 and p=0.865, respectively; K-W tests; **Figure 1J** and **Online Table S1**). This data demonstrate that the cerebellar projection innervates preferentially VL and that their terminals are not only more abundant, but also bigger compared to VM and CL.

Basic transmission properties of cerebello-thalamic synapses differ across thalamic nuclei

It has been shown by sharp electrode recordings in anesthetized cats and rats that electrical stimulation of the cerebellar nuclei axons could elicit monosynaptic excitatory post-synaptic potentials (EPSPs) from which a fast spike could arise in VL relay cells [91, 92]. To our knowledge, no data have been published about the postsynaptic currents underlying these changes in VL potentials, or about the postsynaptic responses of thalamic VM or CL cells. To gather these data we performed whole cell patch-clamp recordings of VL, VM and CL neurons in acutely prepared thalamic slices that contained YFP-labelled, ChR2-expressing CN axons (see material and methods section). Overall, we found that the resting membrane potential of VL (-71.6±0.9 mV), VM (-72.2±2.0 mV) and CL (-70.0±1.4 mV) neurons was not significantly different (p=0.736, one-way ANOVA), but that the input resistance of CL neurons was significantly higher than in VL neurons (p=1 for VL *vs* VM, p=0.012 for VL *vs* CL and p=0.175 for VM *vs* CL; n=49; K-W test). In all three thalamic nuclei single light pulses (1 ms, 470 nm, applied through the objective) elicited an EPSC (**Figure 2A**).

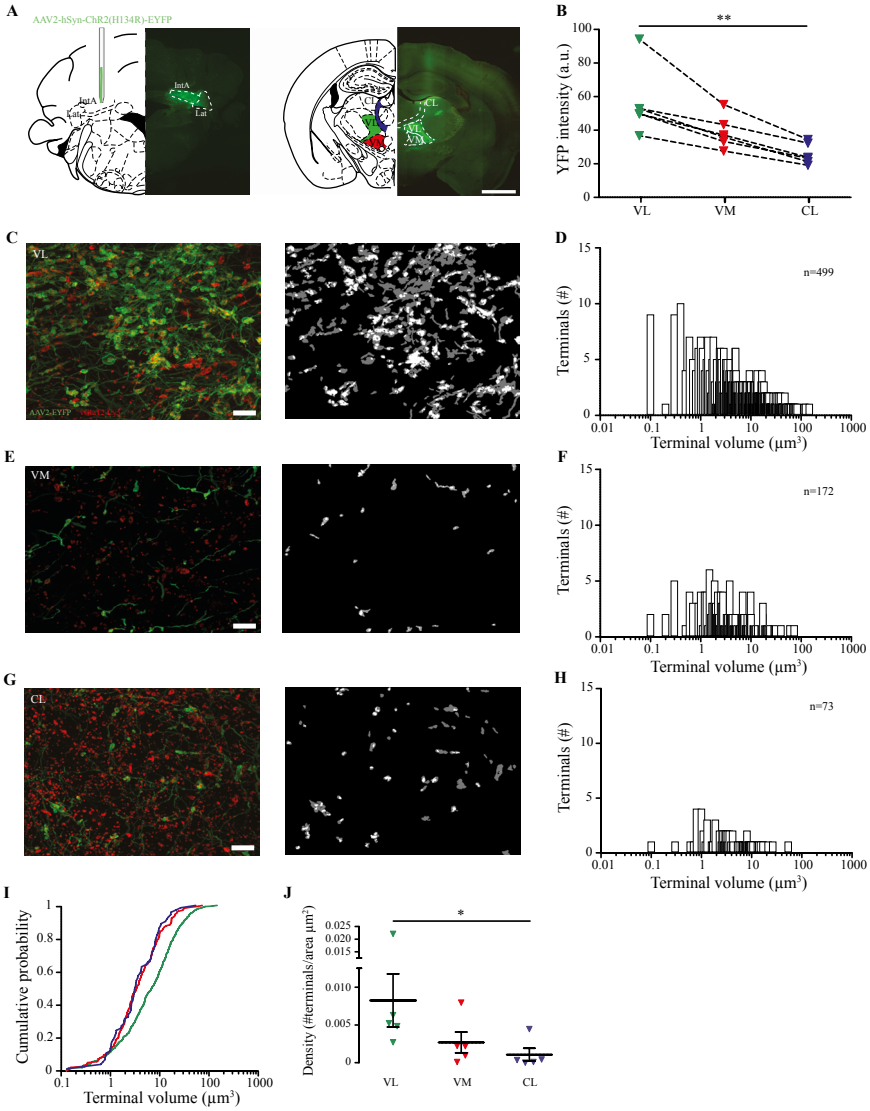

Figure 1. Variable innervation of VL, VM and CL nuclei by CN axons.

A schematic representation of the experiment. (left) AAV-injection in the interposed nucleus and (right) fluorescent (ChR2-EYFP) CN axons throughout the thalamic complex (3 weeks post-injection). The nuclei of interest are highlighted in green (VL), red (VM) and blue (CL). This color code will be applied throughout all the figures. Scale bar indicates 1 mm. ***B*** percentage of YFP signal in the three nuclei of interest (N = 6 mice) normalized to fluorescence in VL. ***C,E,G*** (left) maximum intensity projection of *Z-stack* (14 µm thick) showing in green ChR2-EYFP stained CN axons, in red vGluT2 staining and (right) the result of the colocalization mask; gray indicates ChR2-EYFP-stained axons and white vGluT2-staining. ***D,F,H*** histograms showing terminal volume and number for VL, VM and CL (N = 5 mice). ***I*** cumulative plot of the terminal volume (green: VL; red: VM; blue: CL). (VL vs CL $p<0.001$: VL vs VM $p<0.001$ and VM vs CL $p=0.966$; N = 5 mice, K-S test). ***J*** Average density of vGluT2-stained CN terminals (VL vs CL $p=0.024$). Data are presented as mean ± S.E.M; * $p<0.05$, *** $p<0.001$. K-W test was used. For full statistical report see Online Table 1.

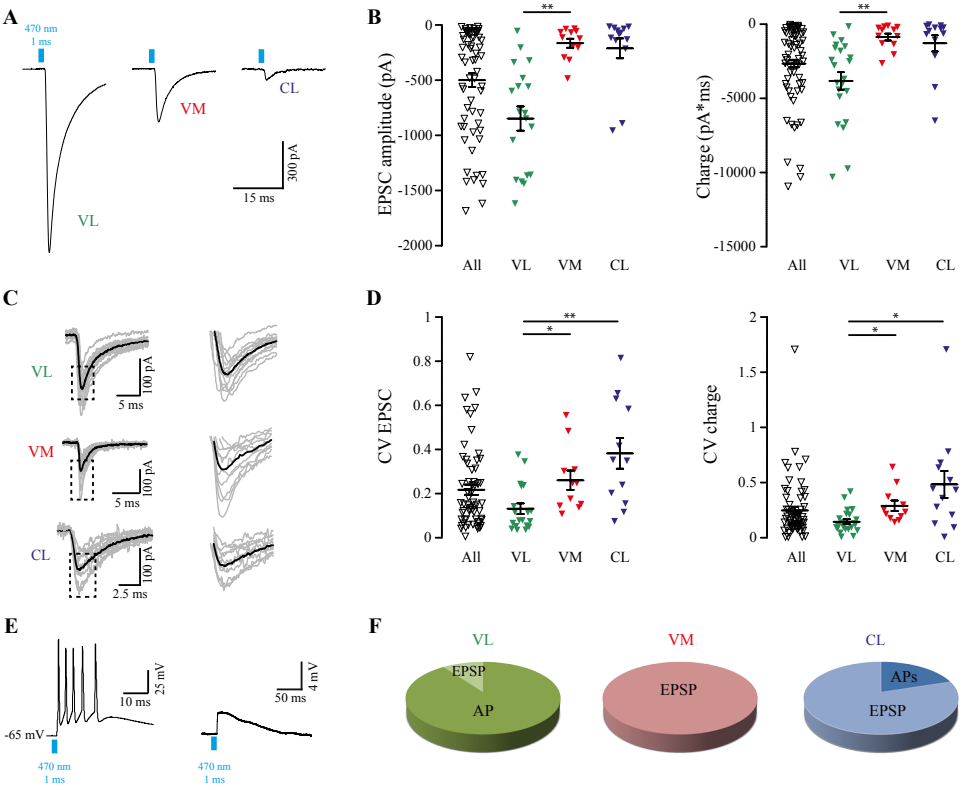

Figure 2. Charge transfer between CN axons and thalamic neurons differs for VL, VM and CL.

A, optical wide field stimulation of CN terminals (470 nm, 1 ms pulse length) evoked EPSCs of variable amplitude in VL, VM and CL. ***B*** quantification of EPSCs amplitude and charge for all recorded cells (n = 63 for EPSC amplitude and n = 65 for charge) and for the nuclei of interest (EPSC: VL: n = 19; VM: n = 12; CL: n = 13; charge: VL: n = 22; VM = 12; CL = 13 respectively; 'All' category represents all cells recorded, of which some were not recovered by histology and therefore were not classified to a specific nucleus – note that all cells in VL, VM and CL are also represented in 'All'). ***C*** example traces of EPSCs amplitude in gray and average trace in black. Note the variability in EPSC amplitude of individual responses. ***D*** coefficient of variation (CV) for (left) EPSCs amplitude and (right) EPSC charge. ***E*** example traces of (left) action potential (AP) firing or (right) excitatory postsynaptic potential (EPSP) evoked by single pulse CN stimulation. ***F*** Pie charts representing responses to CN stimulation recorded in current-clamp mode (VL: n = 9 AP, n = 1 EPSP; VM: n = 3 EPSP; CL: n = 1 AP, n = 4 EPSP). Data are presented as mean ± S.E.M; * $p<0.05$, ** $p<0.01$, *** $p<0.001$. K-W was used. For full statistical report see Online Table 2.

These events were reliably blocked by bath-application of the voltage-gated Na^+-channel blocker tetrodotoxin (TTX) (n = 5 cells; >99% decrease in charge transfer), which indicates that the postsynaptic events were triggered by action potential-driven release of glutamate from CN terminals. The mean EPSC amplitude that we could maximally evoke was significantly higher in VL than in VM and CL (VL: -847.7 ± 109.5 pA; VM: -165.0

± 40.2 pA; CL: -210.8 ± 89.2 pA; p=0.001 for VL *vs* VM, p<0.001 for VL *vs* CL and p=1 for VM *vs* CL; K-W tests), which was also represented in the evoked charge (VL: -3820 ± 595 pA*ms; VM: -862 ± 235 pA*ms; CL: -1284 ±542 pA*ms; p=0.002 for VL *vs* VM; p=0.001 for VL *vs* CL, p=1 for VM *vs* CL; K-W tests; **Figure 2B** and **Online Table S2**). The variability in optically stimulated EPSC amplitude and charge was quantified by calculating the coefficient of variation (CV) (**Figure 2C**). We found significant differences in the CV of EPSC amplitudes (VL: 0.13 ± 0.02; VM: 0.25 ± 0.04; CL: 0.38 ± 0.07; p=0.031 for VL *vs* VM, p=0.001 for VL *vs* CL; p=1 for VM *vs* CL, K-W tests, Dunn's correction; **Figure 2D** and Online Table S2) and of EPSC charge (VL: 0.13 ± 0.02; VM: 0.28 ± 0.04; CL: 0.47 ± 0.12; p=0.03 for VL *vs* CL, p=0.025 for VL *vs* VM, p=1 for VM *vs* CL, K-W tests, Dunn's correction and Online Table S2). We found no significant correlation of the incubation time to the EPSC amplitude, nor to the CV of the EPSC amplitude (p=0.470, r_s=0.116 for EPSCs and p=0.269, r_s=0.161 for CV, Spearman correlation), which supports the notion that the difference in postsynaptic responses is actually due to a difference in the charge transfer between CN axons in VL, VM and CL neurons.

To establish the impact of neurotransmitter release from CN terminals on thalamic neurons' membrane potential we also recorded a subset of cells in current clamp (**Figure 2E**). When stimulated at maximum light intensity most VL neurons fired action potentials (9 cells out of 10) whereas most VM (3 out of 3) and CL neurons (4 cell out of 5; **Figure 2F**) were not able to elicit action potential firing. The probability to elicit an action potential was not related to the resting membrane potential of the cell (p=0.628; r_s=-0.127, Spearman correlation). As we expected from the EPSC amplitudes, neurons in VL fired action potentials more readily than those in VM and CL.

Thalamic responses show paired-pulse depression and are predominantly sensitive to ionotropic glutamate receptor blockers

Thalamic afferents are often categorized as 'driver' or 'modulator' [150, 393]. This classification is partially determined by the response to repetitive stimulation of presynaptic terminals: driver synapses are thought to show paired-pulse depression (PPD) whereas modulator synapses evoke paired-pulse facilitation (PPF) [394-396]. Although cerebellar input to motor thalamus has been listed as driver input [150], short-term synaptic dynamics of thalamic responses following repetitive CN stimulation in VL, VM and CL still need to be evaluated. Here we performed voltage-clamp recordings while stimulating the CN terminals repetitively with trains of light pulses at 10, 20 and 50 Hz (**Figure 3A-C**). To evaluate the time course of the depression we normalized EPSC amplitudes to the first peak amplitude (**Figure 3D-F**).

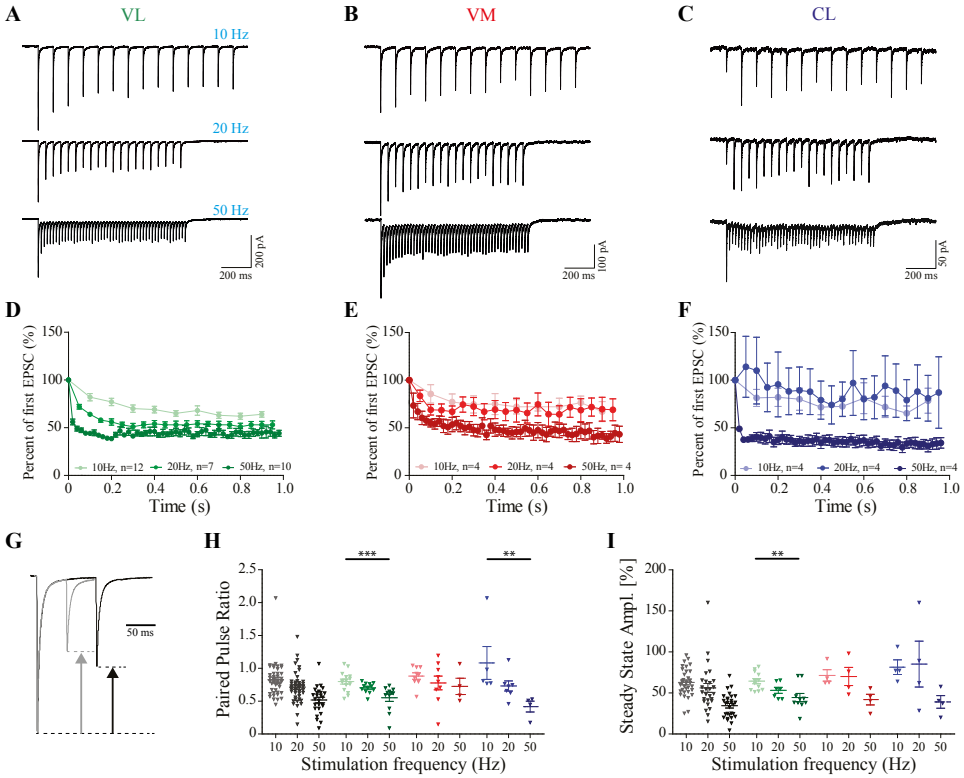

Figure 3. High-frequency stimulation results in paired-pulse depression of EPSC.

A,B,C Averaged responses of VL, VM and CL neurons (of 5 repeats) to 1 sec trains of 10 Hz, 20 Hz or 50 Hz stimuli. ***D,E,F*** Average normalized EPSC amplitudes for 10, 20 and 50 Hz stimulus trains. ***G*** superimposed example responses (average of 5 repeats) to paired-pulse stimulation at 10 Hz (black) and 20 Hz (grey). ***H*** average paired pulse ratio at 10, 20 and 50 Hz for each recorded cell in each nucleus. ***I*** average normalized steady state response amplitude during the last 5 stimuli of the train for each cell in each nucleus. (For panels H and I: VL: n=29; VM: n=12; CL: n=12) ** $p<0.01$, *** $p<0.001$. For full statistical report see Online Table 3.

In general, we found that the ratio between the amplitudes of the first two EPSCs showed a PPD at all frequencies tested (**Figure 3G**). At 50 Hz the second EPSC showed a twofold reduction in amplitude compared to the initial one (VL: 0.52 ± 0.06; VM: 0.72 ± 0.12; CL: 0.41 ± 0.08), whereas lower frequency stimulations showed a smaller effect on the paired-pulse depression. At 20 Hz the depression was around 30% of the first EPSC in all the nuclei (VL 0.70 ± 0.02, VM 0.77 ± 0.10, CL 0.73 ± 0.07) whereas at 10 Hz only VL (0.80 ± 0.03) and VM (0.88 ± 0.04) neurons showed on average PPD but CL did not (1.08 ± 0.25) (**Figure 3H**). When we compared the paired-pulse depression across all nuclei for each frequency, we found that the ratio between the first two responses did not show any

significant difference between the nuclei (10 Hz: p=0.344; 20 Hz: p=0.168; 50 Hz: p=0.137, K-W tests, Dunn's correction; **Figure 3H** and Online Table S3).

Next, we analyzed the subsequent responses to the train stimulation to determine the average sustained release of presynaptic terminals during high frequency steady-state synaptic transmission (**Figure 3A**). For this analysis, the average phasic EPSC amplitude within the train was normalized to the average first EPSC amplitude for each frequency and each nucleus. Across all recorded cells, we find normalized steady state amplitudes of 64.4 ± 3.1% (VL), 71.3 ± 6.9% (VM) and 81.4 ± 8.9% (CL) at 10 Hz: 53.1 ± 3.6% (VL), 70.1 ± 11.1% (VM) and 85.2 ±28.0% (CL) at 20 Hz and 44.4 ± 5.0% (VL) 41.9 ± 6.5% (VM) and 39.1 ± 7.7% (CL) at 50 Hz (**Figure 3I** and Table S3). We found no significant differences between the values recorded per nucleus, but did find that in VL the steady-state depression was significantly higher at 50 Hz than at 10 Hz (p =0.005, K-W test, **Figure 3I** and Table S3). These data indicate that the general tendency for transmission at cerebello-thalamic synapses in VL, VM and CL is to show a depression of neurotransmitter release in response to repetitive stimulation.

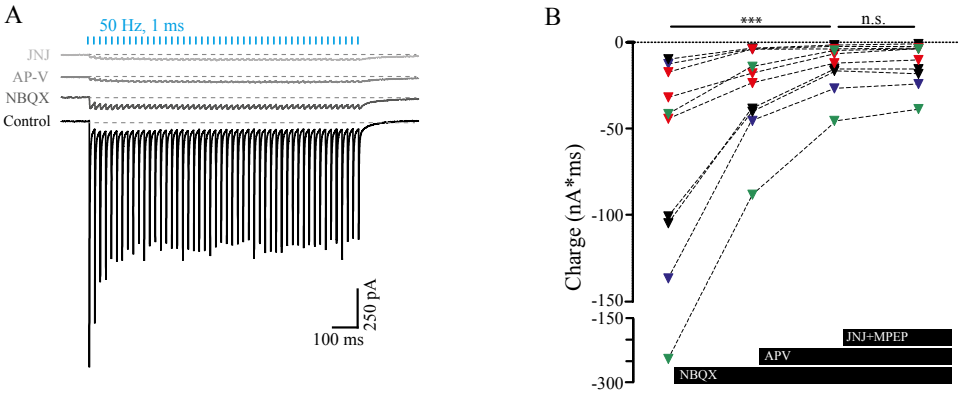

Figure 4. Thalamic responses to CN-stimulation are sensitive to ionotropic receptor blockers.

A example traces of averaged EPSCs evoked by 1 sec train of 1 ms pulses at 50 Hz in control (ACSF) conditions and following application of NBQX, APV and JNJ+MPEP to block AMPA, NMDA and mGluR1 and 5 receptors, respectively. ***B*** summary data showing the decrease of charge after drugs application (VL in green, VM in red, CL in blue, undefined location in black;n=10 in total). *** p<0.001. For full statistical report see Online Table 4.

Our results indicate that the synaptic transmission at cerebello-thalamic synapses in VL, VM and CL are glutamatergic, which matches previous *in vivo* findings on the excitatory responses of VL neurons evoked by microstimulation of the brachium conjunctivum or the neurons in CN [91, 92, 380, 389]. To elucidate whether these excitatory postsynaptic

responses where mediated by ionotropic and/or metabotropic receptors we next tested the effects of their selective blockage on the responses to 50 Hz stimulus trains. Upon wash-in of AMPAR-antagonist NBQX the EPSC charge decreased from -74.6 ± 2.4 nA*ms to -28.0 ± 8.3 nA*ms and following the wash-in of NMDAR-antagonist APV the EPSC charge decreased even further to -13.5 ± 4.3 nA*ms (p<0.001, Friedman test; **Figure 4A-C** and Online Table S4). Further application of blockers for the mGluRs most abundantly expressed in thalamic neurons (JNJ for mGluR1 and MPEP for mGluR5 [395, 397] did not affect the remaining current (-12.1 ± 3.9 nA*ms; Friedman test, p=1; **Figure 4D** and Online Table S4), suggesting the absence of a substantial mGluR1- or mGluR5-mediated component in cerebellar transmission on thalamic neurons.

Postsynaptic determinants of variable CN-impact in thalamic cells

Next we evaluated whether the electrophysiological characteristics described above could be linked to the morphology of the thalamic neurons, bearing in mind that in rat thalamus the neuronal morphology in VL, VM and CL neurons varies [367-370, 373, 381, 398]. By reconstructing biocytin-filled neurons throughout the VL, VM and CL nuclei (**Figure 5A**) and analyzing their dendritic branching using a 3D-Sholl analysis (**Figure 5B**) we found that 23 VL neurons on average show a more elaborate branching pattern than the 14 CL neurons at 55 μm distance from the soma (p<0.05, 2-way ANOVA; Mann Whitney comparison, **Figure 5C,D** and Online Table S5). The number of proximal dendrites (VL: 8.13 ± 0.47; VM: 7.83 ± 0.83; and CL: 6.83 ± 0.34) was not significantly different between nuclei (p=0.115, K-W test; **Figure 5E** and Online Table S5). To better illustrate the dendritic architecture of cells in each of the three defined nuclei we also quantified the radial distance between dendrites at 15 μm from the soma. We found no significant difference in the distance (VL: 40.2 ± 2.6 degrees; VM: 41.1 ± 3.5; CL: 47.0 ± 2.8; p=0.14, K-W test; **Figure 5F,G** and Online Table S5). Although limited, these morphological distinctions between the neurons in VL, VM and CL in combination with the electrophysiological characteristics, suggest differential impact of cerebellar input to thalamic neurons.

Distribution and morphology of reconstructed CN terminals

Previous anatomical studies in rats suggested that in VL cerebellar terminals are larger than those in intralaminar nuclei [84]. To further characterize the identity of cerebellar terminals that we optogenetically stimulated, we stained the slicing containing the patched neurons for VGluT2 and assessed the morphology of the cerebello-thalamic contacts for each recorded neuron using high magnification confocal microscopy (**Figure 6A**).

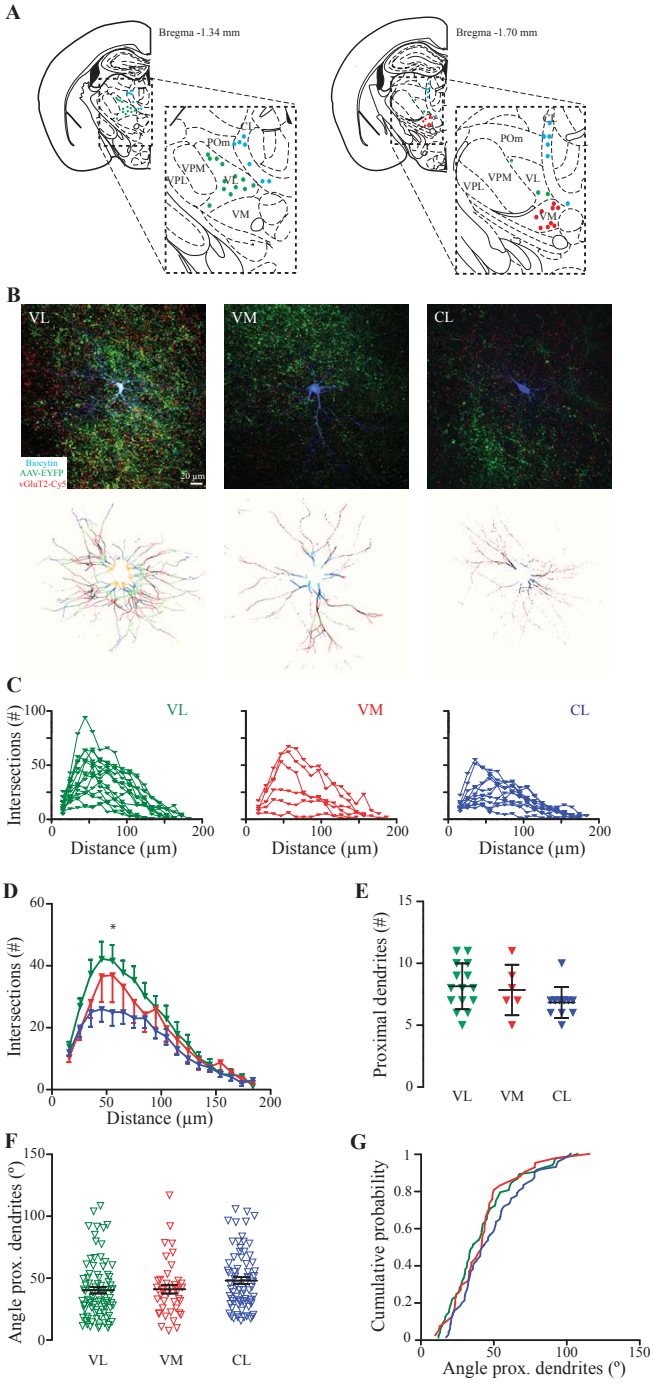

Figure 5. Morphological characterization of thalamic cells recorded in VL, VM and CL.

A Location of all recorded cells in VL, VM and CL projected on two coronal planes [422] ***B*** (top) maximum projections of the somatodendritic morphology of biocytin-filled cells (blue), surrounding ChR2-EYFP labelled CN axons (green) and vGluT2-staining (red) for VL (left), VM (middle) and CL (right). (bottom) maximum projections of 10 µm-thick 3D-spheres surrounding an example neuron from VL, VM and CL (as indicated by the different colors along dendritic trees). ***C*** Sholl analysis shows dendritic arborisation by the number of intersections of the concentric spheres for VL (left), VM (middle) and CL (right) (VL: n=15; VM: n=6; CL: n=11). ***D*** average number of dendritic intersections is shown in 10 µm steps from the soma and each nucleus. ***E*** number of proximal dendrites as quantified at 15 µm distance from soma for VL, VM and CL (VL: n=15; VM: n=6; CL: n=11). ***F*** directionality of proximal dendrites (at 15 µm from soma center) determined by the angle between individual dendrites. Note that the angle is proportional to the angular distance between two neighboring dendrites. ***G*** cumulative distribution of data represented in panel *F*. * $p<0.05$, ** $p<0.01$. For full statistical report see Online Table 5.

The number of vGluT2-positive CN axon terminals on the recorded cells did not vary significantly between the nuclei (VL: 4.5 ± 0.7; VM: 3.66 ± 1.17; CL: 3.08 ± 0.83; p=0.37, K-W test, **Figure 6C**, Online
Table S6) neither their distance from soma (VL: 26.7 ± 1.9 µm; VM: 33.8 ± 5.7 µm; CL: 26.6 ± 2.5 µm; p=0.58, K-W test, **Figure 6D**; Online Table S6). To enhance the *x-y* resolution and reduce the blurring caused by the point spread function, we deconvolved the images and selected the vGluT2-positive terminals to measure their volume (**Figure 6B**). We found that terminals onto recorded VL neurons had a larger volume (11.67 ± 1.30 µm^3) than those onto recorded CL neurons (CL: 7.23 ± 1.57 µm^3) (p=0.02, K-W test, **Figure 6E-F** and Online Table S6), whereas no significant differences were found comparing VM terminals (9.26 ± 1.93 µm^3) to VL and CL (p=1.00 and p=0.35, respectively, K-W tests, **Figure 6E-F** and Online Table S6).
To further investigate CN axon terminal dimensions and characteristics of the post-synaptic structures we studied synaptic contacts at the ultrastructural level. Representative examples of the synaptic profiles formed by BDA-stained CN axons and thalamic neurons are shown in **Figure 7A**. Measurements made from the profiles included terminal surface, number and size of mitochondria, dendritic diameter, PSD length and number of release sites per terminal (**Figure 7B**). Although we observed in the fluorescent images that the terminal size was significantly different between VL and CL, at the ultrastructural level the difference was not significant even though on average VL terminals appeared to be bigger (VL: 2.35 ± 0.38 µm^2; VM: 2.07 ± 0.31 µm^2; CL: 1.23 ± 0.11 µm^2 p=0.099, K-W test). We did observe a significant difference in the mitochondrial surface between VL and CL (VL: 0.13 ± 0.01 µm^2; VM: 0.10 ± 0.01 µm^2; CL: 0.06 ± 0.005 µm^2; VL vs VM p=0.034; VL vs CL $p<0.001$; VM vs CL $p< 0.001$; K-W test; **Figure 7B** and Online Table S7). Another characteristic of cerebello-thalamic synapses we could observe in all three nuclei is that most terminals contained several release sites (VL: 2.97 ± 0.38; VM: 3.08 ± 0.47; CL: 2.96 ± 0.29; p=0.667; K-W test) [348].

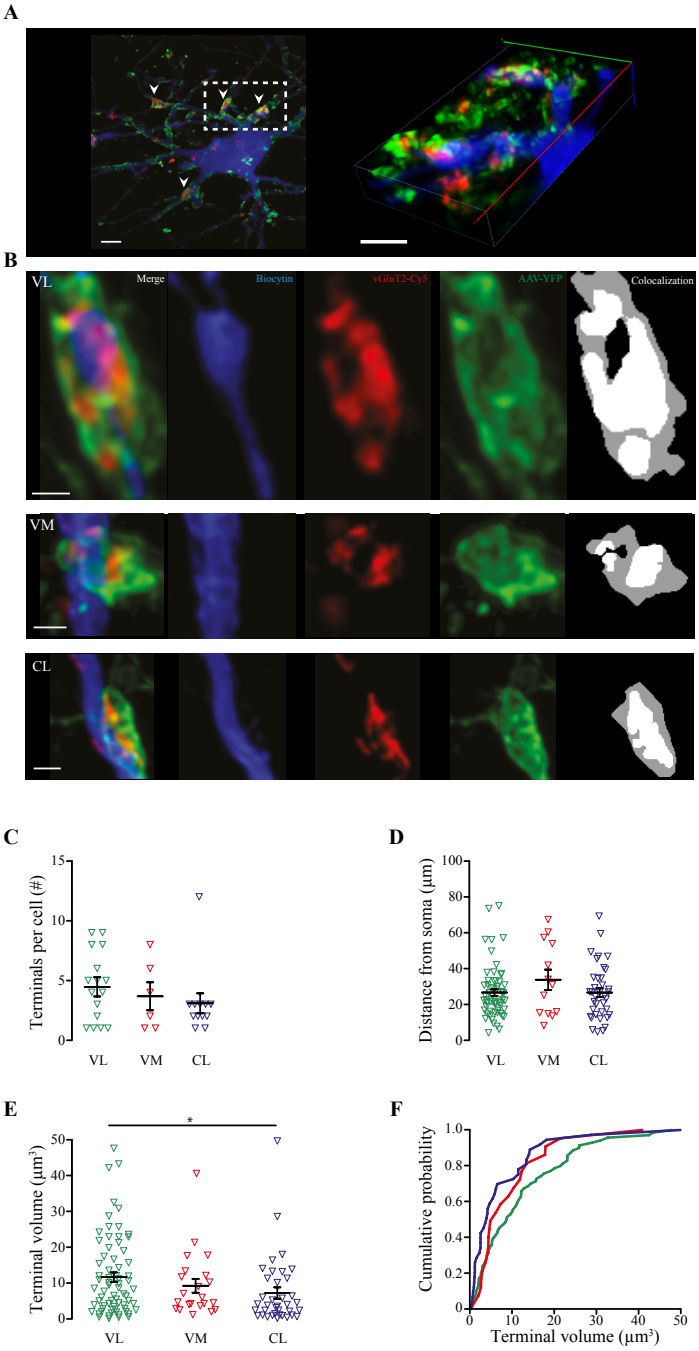

Figure 6. CN terminals of variable volume are similarly positioned along dendrites of recorded thalamic neurons.

A maximum intensity projection of Z-stack image (22 µm thick) of biocytin filled neuron (blue: streptavidin-Cy3; green: ChR2-YFP terminals; Red: vGluT2-Cy5. Arrowheads indicate the vGluT2-positive terminals onto proximal thalamic dendrites. ***B*** summary data of reconstructed vGluT2-positive terminals (VL: n = 16; VM: n = 6; CL: n = 12). ***C*** summary data of distance of reconstructed terminals from soma (VL: n = 60; VM: n = 13; CL: n = 37. ***D*** (left four panels) example of isolated terminals (blue: thalamic dendrite; red: vGluT2; green: CN terminal). (right panel) colocalization of ChR2-EYFP and vGluT2-staining to identify active terminals and calculate their volume based on ChR2-EYFP signal. ***E*** terminal volume (VL: n=71; VM n=22; CL n=37). ***F*** cumulative distribution of terminal volume (data as in panel *E*). * $p<0.05$. For full statistical report see Online Table 6.

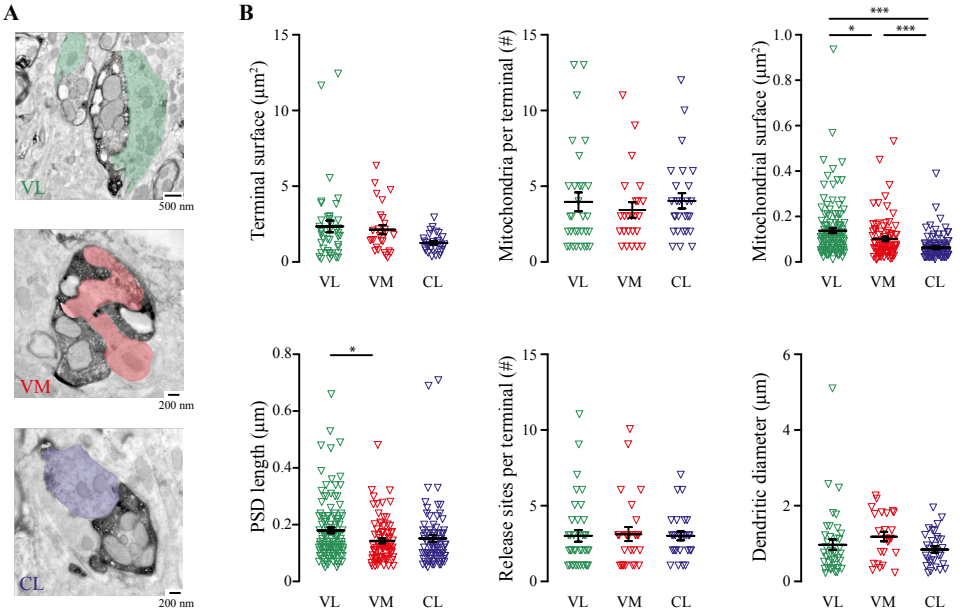

Figure 7. Ultrastructure of CN terminals in VL, VM and CL reveals pre- and post-synaptic specialization.

A Pseudo-colored ultramicrographs of CN terminal in VL (top), VM (middle) and CL (bottom). Note the complex structure of these terminals. ***B*** Quantification of terminal surface (top left; VL: n=48; VM: n=28; CL: n=27, number of mitochondria (top middle; VL: n=32; VM: n=27; CL: n=24;), mitochondrial surface (top right; VL: n=124; VM: n=109; CL: n=82; VL vs VM $p=0.034$; VL vs CL $p<0.001$; VM vs CL $p<0.001$, K-W tests), length of post-synaptic density (PSD) (bottom left; VL: n=114; VM: n=81; CL: n=80; VL vs VM $p=0.024$; VL vs CL $p=0.055$; VM vs CL $p=1$; K-W test), release sites per terminal (bottom middle; VL: n=37; VM: n=27; CL: n=26; $p=0.667$, K-W test) and diameter of the contacted dendrite (bottom right; VL: n=40; VM: n=31; CL: n=25; $p=0.080$, K-W test). * $p<0.05$, *** $p<0.001$. For full statistical report see Online Table 7.

At the post-synaptic side we found that although the dendritic diameter opposing CN terminals did not show any difference between the nuclei (VL: 0.97 ± 0.13 µm; VM: 1.18 ± 0.12 µm; CL: 0.84 ± 0.08 µm; $p=0.08$; K-W test), we did find that length of post-synaptic densities (PSD) were longer in VL (0.17 ± 0.01 µm) compared to VM (0.14 ± 0.01 µm) and CL (0.15 ± 0.01 µm; VL vs VM: $p=0.024$; VL vs CL: $p=0.055$; VM vs CL: $p=1$; K-W

test). Altogether, these ultrastructural findings support the notion that CN axons tend to synapse on proximal dendrites in all three studies nuclei, but that there may be a structural difference in the constellation of the pre- and post-synaptic sites which could correlate to the difference in transmission at CN-synapses throughout the thalamic complex.

Discussion

Our study provides a detailed description of the synaptic transmission at identified cerebello-thalamic synapses in the thalamic VL, VM and CL nuclei onto neurons of which it is known that their axons project throughout various parts and layers of the cerebral cortex, thereby CN axons can exert a strong impact on cortical activity and the encoded behavior. The electrophysiological properties of thalamic neurons in different cerebellar-recipient nuclei were studied with presynaptic optical stimulation and postsynaptic whole-cell recordings. Single-pulse and train stimulation to CN terminals elicited EPSCs of variable amplitudes in thalamic neurons of VL, VM and CL. Still, repetitive stimulation consistently evoked PPD of the responses in VL, VM and CL neurons. The evoked responses in all nuclei were reduced by blockers of ionotropic glutamate receptors, but no further effect was observed upon subsequent application of metabotropic receptors blockers. The differential physiological properties were reflected to some extent by the cellular morphology of VL, VM and CL nuclei as quantified by confocal and electron microscopy.

Our data show that in mouse brain CN neurons innervate the VL thalamic nucleus more densely compared to VM and CL. Although the distribution matches that in other species [89, 348, 362-364, 366, 399, 400] our study does provide one of the first quantitative comparisons of active CN axon terminals in VL, VM and CL, since we exclusively quantified the ChR2-EYFP labeled CN terminals that were co-labeled by vGluT2-staining. Our density values of CN terminals per nucleus (**Figure 1**) may very well be an underestimate given that i) the injections of viral particles did not transfect the complete CN population and ii) the use of vGluT2-antibodies most likely resulted in a limited penetrance into the slices, leaving those CN terminals that are located deeper into the slice unstained. These aspects are also likely to confound the number and location of CN axon terminals on a single thalamic neuron (**Figure 6**) in that there may have been more CN terminals that contributed to the evoked charge transfer, but that due to their location, i.e., depth in the slice, some were identified as vGluT2-negative. Still, we would like to emphasize that the difference in the number of CN terminals between VL, VM and CL is likely to be independent from viral transfection rates or antibody penetrance since these data have been gathered from the

same tissue samples. Our ultrastructural analysis of CN terminals further revealed that, at least for VL, the characteristics described earlier for rat brain, i.e., large terminal surface, fragmented release sites and large diameter of opposing dendritic structure [331, 348, 400], are also found in mouse brain.

The electrophysiological characterization of thalamic responses to CN stimulation revealed that on average VL neurons showed larger EPSCs than those in VM or CL. As expected, these voltage-clamp results translated to a higher chance of action potential firing upon stimulation for VL than for VM and CL when recorded in current-clamp. Our data from VL and VM match earlier reports about faithful action potential firing by VL neurons upon CN or brachium conjunctivum stimulation [91, 92, 349, 380, 389, 401]. Electrophysiological data about CN-CL transmission have not been published before, although recent data indicate that responses of CN neurons to optogenetic stimulation may be faithfully transmitted by CL neurons [256]. Previous electrophysiological data gathered in cats indicate that axons from lateral and interposed CN converge on single VL neurons [106, 389]. Given that our viral transfections reached both lateral and interposed nuclei it may be that at least part of the variability in the recorded responses is due to differential origin of the axons. Yet, to our knowledge no data have been published that suggest a differential impact of lateral and interposed axon terminals on downstream targets.

Referring to intracellular *in vivo* recordings, the cerebellar input on VL neurons has been classified as a driver input to neurons in the motor domain of the thalamus [91, 92, 150]. However, several recent papers classify thalamic inputs in more than two categories: in addition to the 'driver' and 'modulator' inputs a third category of 'driver-like' input has been defined [402]. In the tecto-geniculate system the driver-like inputs have also been identified at the anatomical level by medium-sized terminals that contain round vesicles and innervate proximal dendrites, and at the electrophysiological level stable response amplitudes to trains of stimuli of up to 20 Hz [403, 404]. Our *in vitro* data showed that responses in VL neurons to stimulation of CN terminals meet a number of criteria used to define driver inputs [393]: *i*) CN stimulation evokes a large post-synaptic current that *ii*) is solely mediated by ionotropic receptors and *iii*) depresses upon higher-frequency stimulation, *iv*) CN axons form large synaptic boutons that *v*) contact proximal thalamic dendrites. For CN terminals in VM and CL the categorization is less clear, since these only show some of the 'driver' characteristics. They lack mGluR-mediated transmission and proximal terminal location and their terminal volume is smaller. Moreover, the responses of VM and CL neurons to CN stimulation are significantly smaller, and CL neurons tend to show a stable paired-pulse ratio in response to 10 Hz stimulus trains. At the ultrastructural level, we also found a trend, although not significant, to a reduced terminal surface in CL compared to VL and

a significantly smaller CL mitochondrial surface. Given that previous studies revealed that terminals with larger surface have a higher chance to release neurotransmitter compared to smaller terminals [405-407], our data may at least partially explain why the evoked response amplitude and charge in CL were smaller and more variable (**Figure 2**). Further explanation for the difference in post-synaptic responses to CN stimulation between VL and the other nuclei may come from the difference in PSD length, which previously has been linked to neurotransmission efficacy [408].

Paired-pulse depression is suggested to play an important role in information processing by helping the system to adapt to ongoing levels of activity [395, 409, 410]; this aspect may be of particular interest for cerebellar inputs to thalamic nuclei, since the firing rates reported for CN projections recorded *in vivo* range from ~30-100 Hz (as reviewed by [81]). In our current experiments the ChR2 off-kinetics limited us to stimulus frequencies well below the maximal CN firing rates, which may also have prevented us from recording a significant effect of mGluR-receptor blockage, in that the total mGluR-mediated currents in thalamic neurons evoked by a stimulus frequency of 50 Hz tends to be limited (see also [411]). Therefore, we cannot rule out that the activation of either pre- or postsynaptic modulatory mechanisms have affected the responses we recorded, or those that may be recorded *in vivo*. A dedicated set of future experiments should be designed to study the release probability of individual CN synapses in the thalamic nuclei, the data of which will help to further classify the input of CN terminals to the different thalamic nuclei.

Our findings provide new building blocks to construct the frame of reference for the impact of the cerebellar output on thalamic neurons. Given that mouse thalamus VL, VM and CL are free of interneurons, we argue that all our recordings are from thalamic relay neurons that synapse throughout the various regions of the cerebral cortex. By adapting the classification of relay neurons from rat thalamus (reviewed by [373], our data from VL and VM represent matrix (M)-type neurons and data from CL represent intralaminar (IL)-type, which to some extent is supported by the reduced dendritic branching of CL neurons (**Figure 6**). If we assume that the axonal branching of M- and IL-neurons in mouse brain indeed shows lamina-specific termination as described for rat [367, 368, 370, 412], our data indicate that the information conveyed by M-type neurons in VL will excite corticocallosal or pyramidal tract neurons [413] in the middle and output layers of motor cortices [367] that contribute to initiation of movement [414]. In contrast, M-type VM neurons projections are more dense in layer 1 of widespread cortical areas, including the motor-associated, orbital, cingulate and visual areas in the rat [368], activation which desynchronizes cortical activity patterns [349, 415]. For IL-type CL neurons it has been shown that their axons excite striatal, but also cortical neurons affecting motor, premotor, parietal, prelimbic and

anterior cingulate processing, as well as regulating behavioral arousal levels [256, 416, 417]. Although it remains to be investigated how in *in vivo* conditions thalamic responses may differ between the different types of neurons, our study provides new insights into the diversity of the cerebellar impact on thalamo-cortical networks. Thalamocortical activity exhibits two distinct states, i.e., tonic and burst firing, which are related to different conditions such as waking, non-REM state, slow-wave sleep or even epileptogenic activity [418]. Thalamic afferents, like CN axons, are likely to modulate the activity of thalamo-cortical relay neurons from tonic to burst firing and vice versa. Indeed, single-pulse stimulation of CN neurons efficiently stops thalamo-cortical oscillations in epileptic mutant mice [46]. The underlying mechanism may at least partially depend on the variable impact of CN axons on thalamic neurons, as we showed for VL, VM and CL. Also other synaptic inputs, alike glycinergic or cholinergic projections arising from brainstem [419, 420] or GABAergic projections from substantia nigra [421], may further diversify the cerebellar impact on thalamo-cortical processes throughout the various (non-) motor domains.